JOURNAL OF PETROLOGY

Journal of Petrology, 2021, 1–15
doi: 10.1093/petrology/egab021
Advance Access Publication Date: 8 March 2021
Original Manuscript

OXFORD

Magmatic Water Content and Crustal Evolution Control on Porphyry Systems: Insights from the Central Asian Orogenic Belt

Chao Wu[1,2], Huayong Chen [1,2,*], and Yongjun Lu[3,4,*]

[1]Key Laboratory of Mineralogy and Metallogeny, Guangzhou Institute of Geochemistry, Chinese Academy of Sciences, Guangzhou, 510640, China; [2]CAS Center for Excellence in Deep Earth Science, Guangzhou, 510640, China; [3]Geological Survey of Western Australia, 100 Plain Street, East Perth, WA, 6004, Australia; [4]Centre for Exploration Targeting and Australian Research Council Centre of Excellence for Core to Crust Fluid Systems (CCFS), University of Western Australia, Perth, WA, 6009, Australia

*Corresponding author. E-mail: huayongchen@gig.ac.cn; yongjun.lu@dmirs.wa.gov.au

Received 17 November 2020; Accepted 3 March 2021

ABSTRACT

Porphyry systems, the most important reserves of Cu and Mo with significant Au, are genetically linked to the emplacement of hydrous and oxidized intermediate to acidic magmas, in response to temporal and geochemical evolution of crust in orogenic terranes. In this study, comprehensive whole-rock and zircon geochemical and isotopic datasets of intermediate to acid igneous rocks were integrated to characterize the crustal evolution and metallogeny of porphyry deposits in the Central Asian Orogenic Belt (CAOB).

The ore-forming porphyries of Cu ± Au ± Mo and Mo deposits have higher but largely overlapped ΔFMQ (the proxy for oxygen fugacity) with those of the barren igneous rocks. However, the ore-forming porphyries of Cu ± Au ± Mo deposits are characterized by distinctly higher whole-rock V/Sc and zircon Eu/Eu* (both are proxies for water content) than barren rocks. Furthermore, the V/Sc ratios positively correlate with the Cu tonnages of calc-alkali porphyry Cu deposits, suggesting that magmatic water contents may yield the first-order control on metal endowment. The general decrease of V/Sc from the Paleozoic to Mesozoic, combined with the negative correlation of V/Sc with K_2O and SiO_2, also indicates the gradual evolution of crust in CAOB clearly controls the end members of porphyry-type systems (i.e., Cu–Au and Mo deposits). The crustal residence age (T_{Res}, the time difference between Nd depleted-mantle model age and the crystallization age) of c. 500 Ma from the Nd isotopes is proposed as the threshold distinguishing porphyry Cu ± Au ± Mo ($T_{Res} <$ 500 Ma) and Mo deposits ($T_{Res} >$ 500 Ma) in the CAOB.

The coupled zircon Hf isotopes and crustal thickness reveal that the fundamental crustal architecture in the eastern and western CAOB had been built by the Late Permian and Late Carboniferous, respectively, highlighted by the converging trends of εHf(t) commencing at *c.*250 Ma in the eastern segment and *c.*300 Ma in the western segment of CAOB, indicating reworking and homogenizing of juvenile crust after collision. In the eastern CAOB, porphyry Cu ± Au ± Mo deposits were formed by juvenile materials in thin island arcs, while porphyry Mo deposits were formed by reworked materials in the thickened orogenic crust after *c.*250 Ma. In the western CAOB, porphyry Cu deposits in the Balkhash region during the Late Carboniferous were formed in thickened continental crust (generally > 40 km), genetically linked to the culmination of world-wide magmatic addition rates (MARs) triggered by accelerated production of the juvenile crust, in contrast to the porphyry Cu ± Au ± Mo deposits formed in thin island arc (generally < 40 km) during the Early Paleozoic.

This study tests the zircon ΔFMQ as proxy for fO_2, and zircon Eu/Eu* and whole-rock V/Sc ratios as proxy for water content. It highlights that whole-rock V/Sc ratio is a favorable index for the

Cu tonnages of porphyry Cu ± Au ± Mo deposits, and that the distinct porphyry-type mineralization in the CAOB is controlled by the crustal evolution reflected by crustal composition and thickness.

Key words: magmatic water content; crustal evolution; porphyry systems; Central Asian Orogenic Belt

INTRODUCTION

The porphyry-type deposits presently contain the world's major Cu and Mo reserves, as well as a significant amount of Au (Cooke *et al.*, 2005; Seedorff *et al.*, 2005; Sillitoe, 2010), and are genetically linked to porphyry intrusions originated from magma chambers in the upper crust that exsolve S- and metal-rich, aqueous fluids at 5–10 km depth mainly in convergent margins (Candela & Piccoli, 2005; Seedorff *et al.*, 2005; Richards, 2009). Although the variable metal endowment in PCDs remains a subject of debate, it is widely accepted that the causative intrusions are characterized by high oxygen fugacity (fO_2) and water content, which are critical for maximizing the metal concentrations of the exsolved aqueous phase (Richards, 2003; Annen *et al.*, 2006; Loucks, 2014; Lu *et al.*, 2015). The oxidized magmas can extract Cu and Mo from the reservoirs during melting (Mungall, 2002; Jugo, 2009; Lee *et al.*, 2012) and further assimilate sulfides during ascent (Sillitoe, 2010; Wilkinson, 2013). The high fO_2 of magma is conjectured to suppress the segregation of Cu as magmatic sulfide from magma, which otherwise may sequester Cu before its partitioning into the aqueous phase from melt (Sillitoe, 2010), and also make Mo occur mainly as Mo^{6+}, thus preventing the substitution of Mo^{4+} for Ti^{4+} in Ti-bearing minerals such as ilmenite and titanite (Černy *et al.*, 2005).

On the contrary, recent studies have raised doubt on the role of high oxidation state on porphyry-type mineralization (Chiaradia, 2014; Matjuschkin *et al.*, 2016; Zhang & Audétat, 2017; Du & Audétat, 2020). For example, sulfide phases are widely reported in the crustal cumulates, resulting from the enhanced stability of sulfide species in deep- to mid-crustal cumulates even for relatively oxidized (NNO + 2) magmas. Although sulfide saturation could be detrimental to ore-forming potential, the concentration of metals by sulfide melt may be a highly effective mechanism for metal enrichment, as long as the sulfide phases are accessible to subsequent exsolved ore-forming fluid (Halter *et al.*, 2005; Wilkinson, 2013; Chen & Wu, 2020). The recent sulfide pre-enrichment model has inevitably challenged the importance of a highly oxidized PCD ore-forming magma (Chen & Wu, 2020). Traditional PCD metallogenic models propose that the magma needs to maintain a high oxidation state to avoid the early formation of the sulfide phase that scavenges ore-forming elements (Jenner *et al.*, 2010). However, isolated sulfide phases are common in the xenoliths of lower crustal cumulates (Richards, 2009; Hou *et al.*, 2017). Sulfide droplets in the melt inclusions represent the components of the upper crustal magma chamber (Nadeau *et al.*, 2010), suggesting that the sulfide saturation in the magma may be a common phenomenon and not detrimental to copper-ore-forming potential (Du & Audétat, 2020).

High water contents favor the high-pressure saturation of the aqueous phase in magma so as to extract the ore metals efficiently (Rohrlach & Loucks, 2005; Sillitoe, 2010; Loucks, 2014). The zircon, a mineral resistant to hydrothermal alteration or weathering, have been widely applied to investigate crustal evolution (Spencer *et al.*, 2014; Spencer *et al.*, 2019; Hawkesworth *et al.*, 2019), as well as newly proposed magmatic oxybarometer of ΔFMQ values based on trace elements (Loucks *et al.*, 2020). The high whole-rock V/Sc and zircon Eu/Eu* ratios, reflecting the advanced crystallization of hornblende relative to titanomagnetite and suppression of early plagioclase crystallization in hydrous magmas, respectively, have also been proposed to indicate the high water content of magma (Loucks, 2014; Lu *et al.*, 2016; Lu *et al.*, 2019).

Recent studies have put forward that crustal evolution controls the temporal-spatial distribution of porphyry deposits in orogens, e.g. in the Neo-Tethyan orogen in Iran and Pakistan, where the matured magmatic arc system results in evolved, volatile-rich magmas at the late stage of the arc's history in each region, and, therefore, have higher mineralizing potential than the prior arc magmatism (Richards *et al.*, 2012). In addition, crustal thickness has an important impact on magmatic evolution and porphyry Cu mineralization, since the Cu sulfides accumulated at the bottoms of the thickened crust may get re-melted to release the metals for the formation of subsequent porphyry-type deposit (Richards, 2009; Chiaradia, 2014).

The CAOB, one of the largest accretionary orogenic systems in the world, went through horizontal and vertical crustal growth, accompanied by extensive crust-mantle interaction, and formed a series of world-class porphyry Cu and Mo deposits, e.g. Kounrad Cu–Au, Aktogai Cu–Mo–Au, Kal'makyr Cu–Au, Oyu Tolgoi Cu–Au, Caosiyao Mo, and Daheishan Mo deposits (Jahn, 2004; Seltmann *et al.*, 2014; Xiao *et al.*, 2009b; Gao *et al.*, 2018). However, there still lacks a comprehensive understanding of to what extent the high water content and fO_2 of the ore-forming magma depend on each other, and their impact on the metal endowments of porphyry Cu deposits. Moreover, the effect of crust evolution, indicated by crustal composition and thickness,

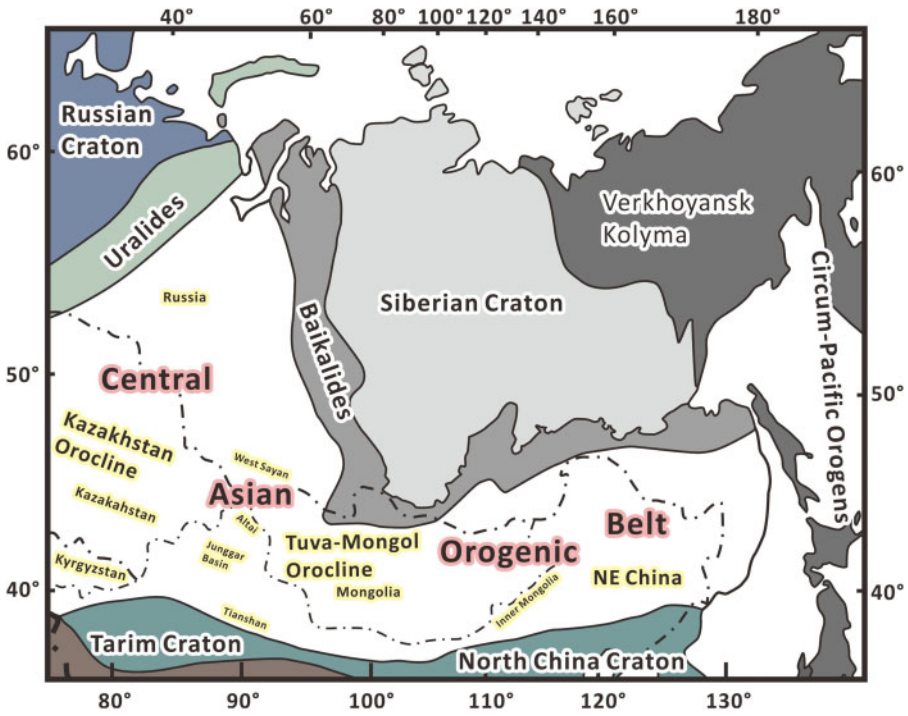

Fig. 1. Simplified tectonic map of the Central Asian Orogenic Belt (Jahn *et al.*, 2000; Jahn, 2004).

on the temporal distribution of porphyry deposits and mineralizing types (e.g. Cu–Au, Cu–Mo, and Mo) remains unclear. Therefore, this paper synthesizes the recent data to characterize the fO_2, water content, Nd isotopes, zircon Hf isotopes and crustal thickness of intrusions from porphyry-type deposits, in comparison to barren igneous rocks in the CAOB, in order to provide the long-term and large-scale overview of the distributions of porphyry-type deposits with respect to the evolution of magmas with increasing crust evolution in the CAOB.

GEOLOGICAL BACKGROUND

The CAOB, extending from the Ural mountains eastwards to the Pacific coast, is bounded by the Russian craton to the west, the Siberian craton to the north, the Tarim and North China cratons to the south (Fig. 1), and mainly formed by subduction and accretion of juvenile materials spanning from the Neoproterozoic to the Mesozoic (Sengör *et al.*, 1993; Jahn, 2004; Yakubchuk, 2004; Windley *et al.*, 2007; Xiao *et al.*, 2009b; Wilhem *et al.*, 2012). The CAOB consists of fragments of ancient microcontinents and a variety of juvenile tectonic units, such as island arcs, oceanic islands, seamounts, ophiolites, and accretionary complexes, preserving various orogenic components, including the Japan-, Mariana-, and Alaskan–Aleutian-type arc systems, as well as the active marginal sequences of cratons (Xiao *et al.*, 2010; Xiao & Santosh, 2014). The CAOB is dominated by the growth and consumption of the Paleo-Asian Ocean (PAO), which was opened in the Neoproterozoic and possibly closed in the Middle Triassic (Wilhem *et al.*, 2012). Two key areas have been well documented in the CAOB, i.e. the Kazakhstan orocline in the west and the Tuva–Mongol orocline in the east (Sengör *et al.*, 1993; Xiao *et al.*, 2010). The Kazakhstan orocline, comprising North Xinjiang in China and Kokchetav-Balkhash in Kazakhstan, is characterized by interactions between the Siberian, East European, and the Tarim cratons in the Late Proterozoic to the Early Mesozoic, while the Tuva–Mongol orocline, comprising Inner Mongolia in China, Mongolia and South Russia, is characterized by convergence in the Early Mesozoic of the Siberian craton, the Mongolia–Gobi block, and the North China craton, as well as the overprinting by the Mongol–Okhotsk and the circum-Pacific orogenesis (Xiao *et al.*, 2010).

The magmatism in the CAOB is characterized by the widely exposed granitoids with positive εNd(t) values, accompanied by multiple phases of alkaline rocks and lesser volumes of mafic–ultramafic magmatism (Han *et al.*, 1999; Jahn *et al.*, 2000; Wang *et al.*, 2017). The massive granitoids occupy a total area more than 8·7 million km^2, clustering into three major periods (i.e. Cambrian–Ordovician, Carboniferous–Permian, and Jurassic) and six peaks of zircon ages at *c.*500, 430–370, 330–300, 290–260, 210–170 and 145–110 Ma (Li *et al.*, 2013; Wang *et al.*, 2017). The granitoids peaking at 500 Ma mainly occur in the northwest CAOB and were formed in subduction and subsequent microcontinental-collision settings (Jahn *et al.*, 2004; Wu *et al.*, 2011), while the granitoids of 430–370 Ma predominately occur in the northwest and south CAOB, and were formed by accretion and collision (Han *et al.*, 2006; Long *et al.*, 2011; Wang *et al.*, 2017). The Carboniferous granitoids in the north and northwest CAOB were formed by post-

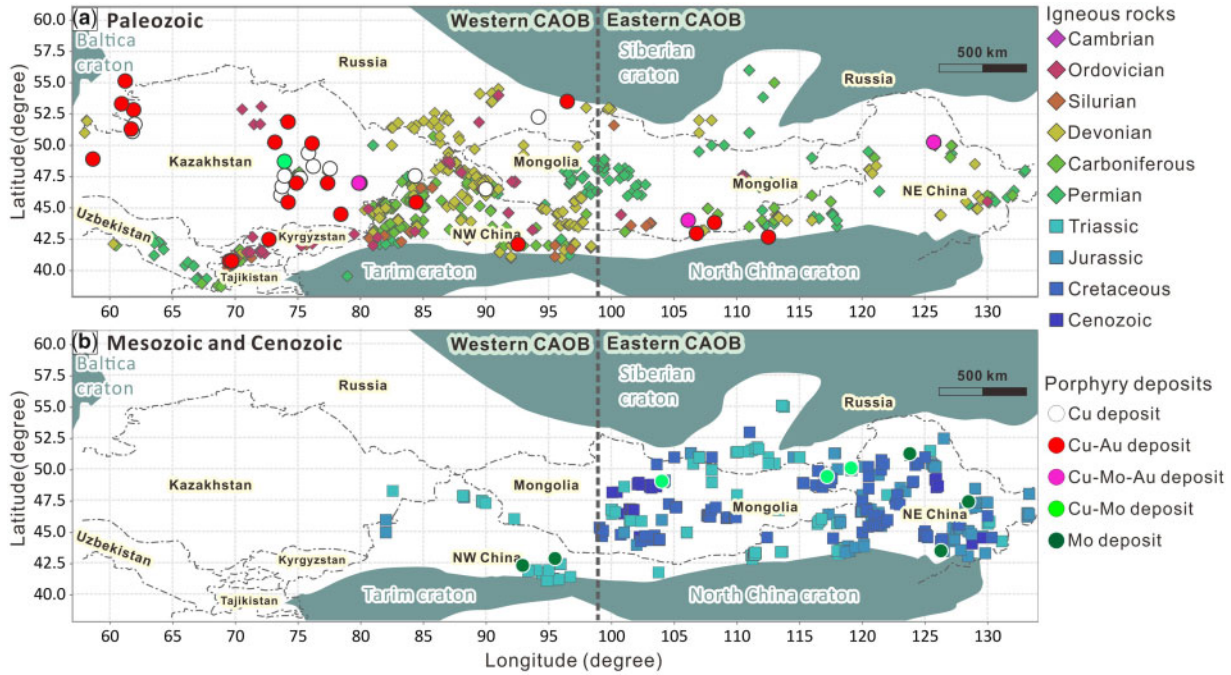

Fig. 2. Distribution map of the magmatic crystallization age for *c.*5000 intermediate to acidic igneous rocks spanning from (a) the Paleozoic to (b) Mesozoic–Cenozoic in the CAOB. Geochronological samples are shown together with the major porphyry Cu and Mo deposits. Note that Mesozoic-Cenozoic rocks (< *c.*250 Ma) are mainly distributed in the eastern CAOB (east of 98° E highlighted by the vertical dashed line).

accretion magmatism, whereas those in the south CAOB were emplaced in an arc setting (Geng *et al.*, 2009; Tong *et al.*, 2015; Wang *et al.*, 2017). The Permian granitoids (290–270 Ma) were formed in various settings, including collisional, post-collisional, and intraplate settings (Wang *et al.*, 2017; Xiao *et al.*, 2009a). The Mesozoic granitoids are mainly present in eastern CAOB (Fig. 2) formed in varying settings (including intraplate, post-orogenic, and continental arc settings) related to three tectonic regimes, namely the consumptions of the PAO, Mongol–Okhotsk Ocean, and Paleo-Pacific Ocean (Mazukabzov *et al.*, 2010; Wu *et al.*, 2011; Xiao *et al.*, 2009a; Li *et al.*, 2013; Gao *et al.*, 2018).

Three porphyry-type mineralizing provinces from the Early Ordovician to the Late Cretaceous are identified in the CAOB (Fig. 2), i.e. the Kazakhstan Cu ± Au ± Mo, the Mongolia Cu ± Au ± Mo and the Northeast China Cu ± Au ± Mo and Mo metallogenic provinces (Yakubchuk *et al.*, 2012; Seltmann *et al.*, 2014; Gao *et al.*, 2018; Shen *et al.*, 2018). The porphyry-type deposits in Kazakhstan cluster at *c.*490–440 Ma and *c.*330–295 Ma, related to the subduction and accretion of Paleozoic arc systems in the western PAO, in contrast to those in Mongolia culminating at *c.*375 Ma and *c.*240 Ma, which are controlled by the evolution of the Gurvansayhan island arc in the PAO and the Selenge continental arc of Mongol–Okhotsk ocean, respectively (Shen *et al.*, 2018). In the Northeast China metallogenic province, the porphyry Cu deposits are represented by the Duobaoshan Cu–Au–Mo deposit at *c.*480 Ma in the Xing'an arc and the Wunugetushan Cu–Mo deposit at *c.*180 Ma in the Debugan collisional zone (Shen *et al.*, 2018). The porphyry Mo deposits in NE China recorded three distinct geodynamic events; i.e. the Triassic deposits distributed along the Xilamulun fault are related to post-collisional crustal extension following the final closure of the PAO; the Jurassic deposits are controversially linked to flat-slab subduction of the Paleo-Pacific oceanic plate or to subduction, collision, and post-collision related to the closure of the Mongol–Okhotsk Ocean; the Cretaceous deposits are attributed to the slab rollback of Paleo-Pacific oceanic plate and lithospheric thinning in Northeast China (Wu *et al.*, 2011; Chen *et al.*, 2017; Shu *et al.*, 2016).

DATA COMPILATION

In order to compare the ore-bearing intrusions of porphyry-type deposits with the immense volumes of barren magmatic rocks, the whole-rock elemental and Nd isotopic data, as well as zircon U–Pb dates of intermediate to acid igneous rocks in the CAOB, were compiled together with their GPS coordinates. The selection criteria for acceptable whole-rock geochemical data are loss on ignition (LOI) < 3·5 wt % to exclude the interference of hydrothermal alteration, and the Eu/Eu* < 1·3 or Al_2O_3 < 20 wt % to exclude conspicuous crystal cumulates, which leaves c.3870 acceptable analyses. Zircon trace-elemental and Hf isotopic data of intermediate to silicic magmatic rocks with available coordinates in the CAOB were also compiled from the literature. The compiled zircon Lu–Hf isotopic dataset includes approximately 12 900 analyses from 800 rock samples. Supplementary Data Tables 1–3; supplementary data

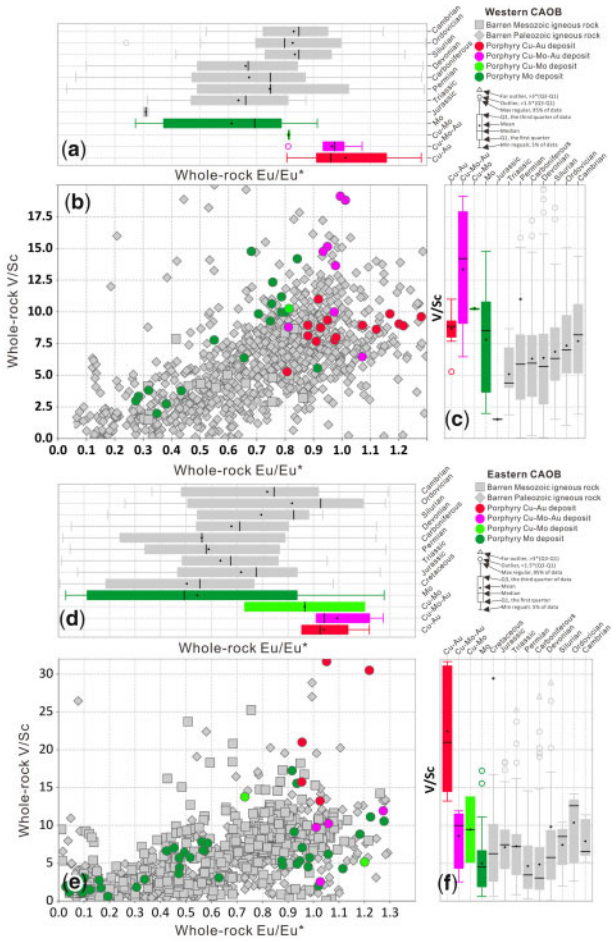

Fig. 3. Whole-rock Eu/Eu* and V/Sc ratios for igneous rocks in CAOB. The rocks from western CAOB are shown in (a) a comparative boxplot of whole-rock Eu/Eu*, (b) binary plot of Eu/Eu* vs V/Sc, and (c) comparative box plot of whole-rock V/Sc. The rocks from eastern CAOB are shown in (d) comparative box plot of whole-rock Eu/Eu*, (e) binary plot of Eu/Eu* vs V/Sc, and (f) comparative box plot of whole-rock V/Sc. The Mesozoic magmatism in eastern CAOB are divided into five groups according to their spatial and temporal distributions because the eastern CAOB went through the impact of three tectonic regimes, including the consumption of the Paleo-Asian Ocean closed up at *c.*250 Ma, the Mongol–Okhotsk Ocean closed up at *c.*170 Ma, and rollback of the Paleo-Pacific Ocean at *c.*130 Ma (Wu *et al.*, 2011; Shu *et al.*, 2016; Chen *et al.*, 2017).

are available for downloading at http://www.petrology.oxfordjournals.org present the complete dataset. The deposit-size criteria in this study for the porphyry Cu–Au and Cu–Mo deposits are based on the metal reserves and grades, with details provided in Supplementary Data Document and Supplementary Data Table 5.

DISCUSSION

Porphyry Cu mineralization correlated with magmatic water content and oxygen fugacity

As illustrated in Figure 3, the whole rock Eu/Eu* ratios demonstrate a broad positive correlation with V/Sc ratios, with the majority of ore-bearing intrusions of porphyry Cu ± Mo ± Au deposits characterized by V/Sc ≥ 10 and Eu/Eu* ≈ 1 in both eastern and western CAOB, which is consistent with the trend for global porphyry Cu deposit (Loucks, 2014; Lu *et al.*, 2015). The whole-rock V/Sc and Eu/Eu* have been widely used as the proxy for the water content of magma, since high magmatic water contents (> 4 wt %) in melt will result in early fractionation of hornblende but suppression of plagioclase crystallization at crustal depths (Richards, 2011; Loucks, 2014).

Recent research has proposed zircon Eu/Eu* (mainly proxy for water content) as the best fertility indicator for PCDs in both Archean and Phanerozoic terranes (Lu *et al.*, 2016; Lu *et al.*, 2019). A new magmatic oxybarometer has been formulated by Loucks *et al.* (2020) to estimate fO_2 of magma, which uses trace-elemental Ce, Eu and Ti in zircon and excludes the large temperature influence on these ratios by considering the Ti content of the zircons. The plots of calculated zircon Eu/Eu* and ΔFMQ values against whole-rock V/Sc demonstrate that the ore-forming intrusions for porphyry Cu ± Mo ± Au deposits have distinctly higher V/Sc ratios (>10) than the barren igneous rocks (Fig. 4), highlighting the critical role of high magmatic water content in the formation of porphyry Cu ± Mo ± Au deposits. Zircon Eu/Eu* >0·4 generally distinguishes the ore-forming intrusions from barren ones (Fig. 4a), while ΔFMQ for porphyry-type deposits are largely overlapped with those in barren magmatic rocks (Fig. 4b).

The Eu/Eu* of zircon can be influenced by crystallization of REE-bearing phases (Loader *et al.*, 2017; Lu *et al.*, 2019), such as prior or concurrent crystallization of plagioclase will decrease the Eu/Eu* in zircon, while crystallization of titanite and hornblende will lead to elevated Eu/Eu* and low Ta contents (< 0·2 ppm) in zircon. However, most zircons in the CAOB have high Ta contents (> 0·2 ppm; Supplementary Data Table), indicating the minimal influence of titanite. As such, the elevated Eu/Eu* in ore-forming porphyries reflects suppression of plagioclase crystallization due to high magmatic water content (Fig. 4a; Lu et al., 2019). The zircon ΔFMQ values, which are calculated employing the thermodynamic calibration and expected to be a robust parameter for oxidation state of magma, also demonstrate the largely overlap between ore-forming and barren magmatic rocks. This may suggest that the high magmatic fO_2 is not the first-order controlling factor but only one of the prerequisites for forming porphyry-type deposits in the CAOB.

In order to further clarify the effect of magmatic water content on the metal endowment, the median values of V/Sc from ore-forming porphyries are plotted against Cu tonnage of porphyry Cu deposits for which whole-rock V/Sc values are available in the CAOB and the world (Fig. 5a), which are further classified into calc-alkalic and alkalic groups based on whole-rock SiO_2 vs K_2O+Na_2O diagram (Fig. 5b). As illustrated by the dashed lines in Fig. 5a, the porphyry Cu deposits in the CAOB define an exponential correlation between V/Sc

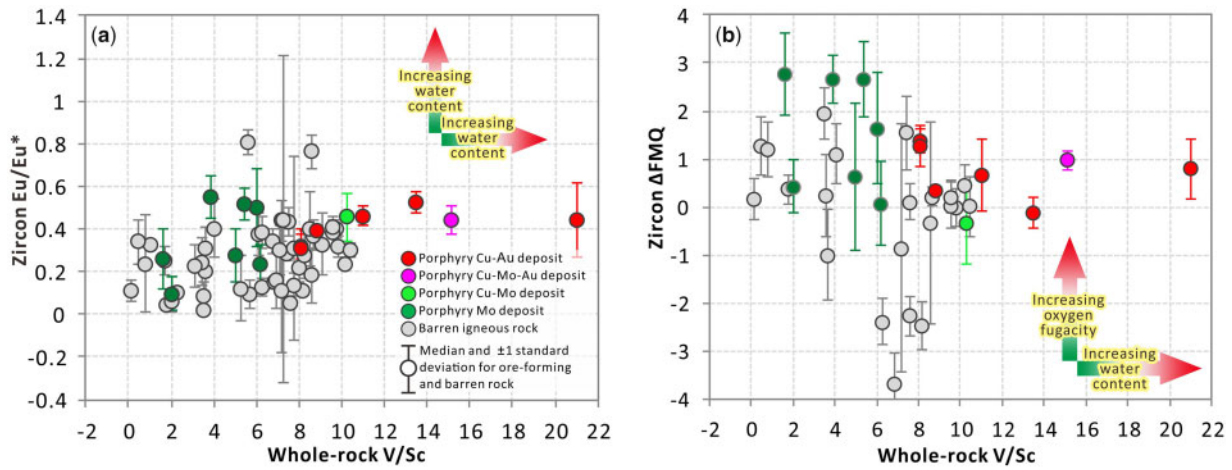

Fig. 4. Whole-rock V/Sc vs (a) zircon Eu/Eu* and (b) ΔFMQ for available barren igneous rocks and ore-forming porphyries in the CAOB, with corresponding medium ± 1 standard deviation of zircon analyses from each sample plotted. The ΔFMQ values are calculated following the approach of (Loucks *et al.*, 2020).

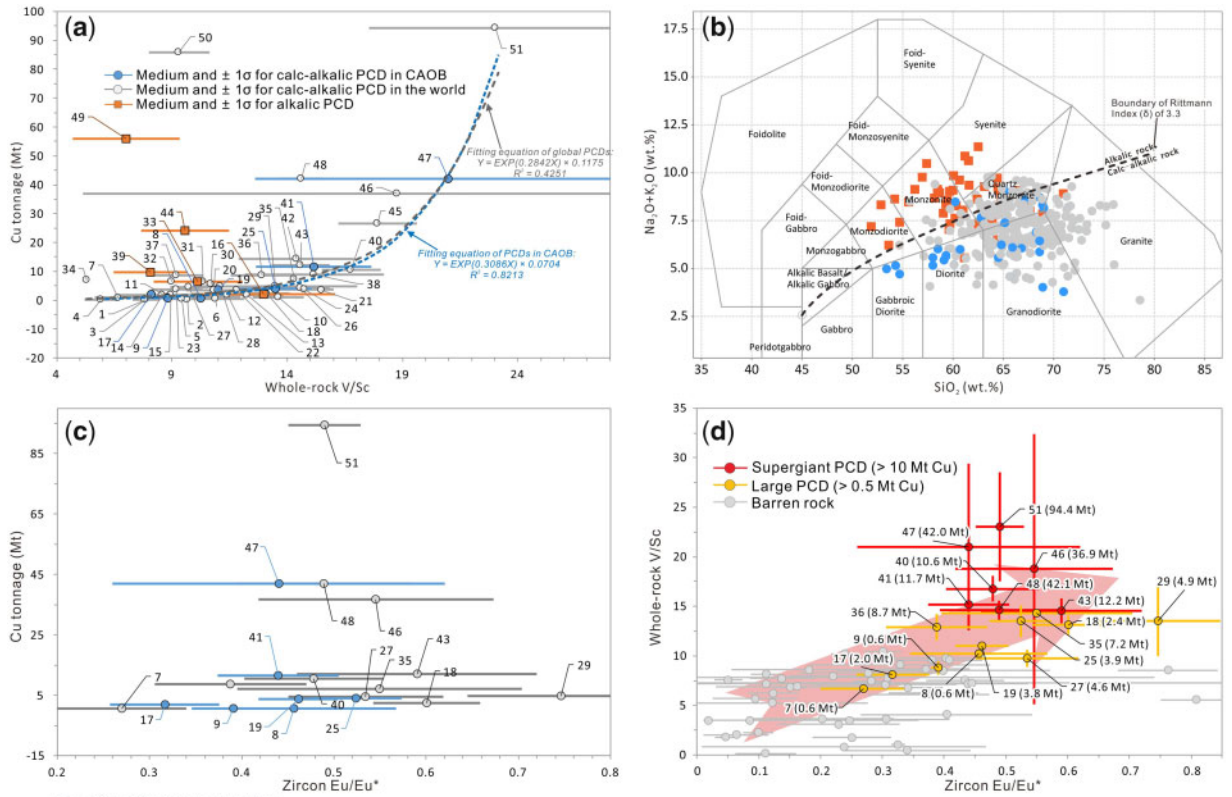

No. of porphyry Cu deposits:
1. Koloula 2. Cash 3. Tameapa 4. Zlatno 5. Contact 6. Copper Creek 7. Copper Canyon 8. Borly 9. Baogutu 10. Mamut 11. Cuatro Hermanos 12. Cobre 13. Silver Bell 14. Taysan 15. Santo Tomas II 16. Skouries 17. Tuwu-Yandong 18. Coroccohuayco 19. Kounrad 20. Schaft Creek 21. Altar 22. Antapaccay 23. El Arco 24. Panagyurishte 25. Nurkazghan 26. Alumbrera 27. Jiama 28. Mission-Pima 29. Sungun 30. Frieda River 31. Quellaveco 32. Inspiration 33. Yulong 34. San Manuel 35. Batu Hijau 36. El Abra 37. Mansa Mina 38. Highland Valley 39. Cadia 40. Qulong 41. Aktogai-Aidarly 42. Santa Rita 43. El Salvador 44. Grasberg 45. Collahuasi 46. Pebble 47. Oyu Tolgoi 48. Chuquicamata 49. Bingham 50. Escondida 51. El Teniente

Fig. 5. Relationship of Cu tonnage with (a) whole-rock V/Sc and (c) zircon Eu/Eu* of ore-forming porphyries from CAOB as well as representative global porphyry deposits. The whole-rock Na_2O+K_2O vs SiO_2 (Middlemost, 1994) and whole-rock V/Sc vs zircon Eu/Eu* of ore-forming porphyries are also shown in (b) and (d), respectively. The Bingham, Grasberg, Cadia, Yulong and Skouries porphyry Cu deposits are classified as alkalic group, while other deposits belong to the calc-alkalic group. Note that Cu tonnages are positively correlated with whole-rock V/Sc ratios for worldwide calc-alkalic porphyry Cu deposits, which define the fitting line (gray dashed line) similar to that derived from porphyry Cu deposits in the CAOB (blue dashed line). Whole-rock V/Sc ratios are positively correlated with zircon Eu/Eu* for both barren rocks and calc-alkalic PCDs, with the latter characterized by higher V/Sc and Eu/Eu* ratios (Fig. 5d). Data sources are provided in Supplementary Data Table 4.

and Cu tonnage with R^2 of 0·82, and global calc-alkalic porphyry Cu deposits, including Batu Hijau, El Teniente, El Salvador, El Abra and Collahuasi, etc, define the similar fitting line defined by CAOB deposits, which independently tests the robustness of such correlation between V/Sc and Cu tonnage (Fig. 5a). By contrast, the alkalic porphyry Cu deposits (e.g. Bingham, Grasberg, Cadia, Yulong, and Skouries) are exceptions, which are off the CAOB fitting line and display overall low V/Sc ratios, suggesting V/Sc ratio is not suitable proxy for magmatic water contents of alkalic intrusions given that elevated K_2O in alkalic melt would destabilize amphibole and decrease the whole-rock V/Sc ratios (Cawthorn, 1976; Loucks, 2014). To the best of our knowledge, this is the first time to quantify the correlation between magmatic water content proxied by whole-rock V/Sc ratio and metal endowment of porphyry Cu deposits. The exponential correlation between V/Sc and Cu tonnage suggests high water content yields a first-order control on forming giant porphyry Cu deposits, a suggestion reinforced by the positive correlation between zircon Eu/Eu* and whole-rock V/Sc (Fig. 5d). Furthermore, the positive correlation between whole-rock V/Sc could be potentially applied to using detrital zircon to footprint the fertile magmatism in large areas. Zircon Eu/Eu* values are not directly correlated with Cu tonnage (Fig. 5c), which combined with the deviation of porphyry copper deposits from the fitting line in Fig. 5a suggest that other factors may also influence the deposit size.

The high water contents of the parental magmas are interpreted to promote the mineralization potential via efficient metal extraction from the magma (Rohrlach & Loucks, 2005) and the formation of stockwork structures into which ore-forming fluids are focused (Zhang & Audétat, 2017). The high water content of ore-forming magma results from either the inheritance from presumably a mantle wedge that has been metasomatized by fluids derived from dehydration of subducting slabs (James, 1981; Leeman, 2001; Plank *et al.*, 2013) or the evolution of magma chamber in lower or upper crust which is recharged with numerous batches of mafic or andesitic magma ascending from mantle wedge or lower crustal depth and forms ore-forming porphyries on the roof (Richards, 2003; Candela & Piccoli, 2005; Wilkinson, 2013; Lee *et al.*, 2014). Previous modeling has described the compositional evolution of magma chambers experiencing simultaneous recharge, evacuation, and fractional crystallization (REFC), which is characterized by pronounced evolution towards enrichments of highly incompatible components, including H_2O and CO_2 (Lee *et al.*, 2014). Some researches put forward that the volume of magma chamber should be 100–200 km^3, based on the estimation of tonnages of porphyry Cu deposits and the average concentrations of ore-forming metals in the parental magma chamber (Zhang & Audétat, 2017). Above all, this study emphasizes the critical role of water content in the magma chamber during the formation of porphyry Cu ± Mo ± Au deposits, which is enhanced in long-lived magma chamber with low rates of evacuation and high mass proportion of recharge (Lee *et al.*, 2014). Besides, the notably low V/Sc ratios for porphyry Mo deposits (Fig. 4), however, do not indicate corresponding low magma water content but the influence of magmatic evolution of Mo-rich magma, which will be discussed in subsequent section.

Controlling of the end-members of porphyry-type deposits

The ore-barren magmatic rocks in the CAOB are characterized by a gradual decrease of V/Sc from the Paleozoic to the Mesozoic, despite the obviously higher ratios in porphyry Cu ± Mo ± Au deposits (Fig. 3c,f). The experimental evidence showed that the elevated content of K_2O present as the molecular component of orthoclase in the melt would destabilize the molecular component of amphibole, thus resulting in the magma experiencing obvious magnetite-induced depletion of V (Cawthorn, 1976; Loucks, 2014; Halley, 2020). Consequently, the whole-rock V/Sc will decrease with the evolution of magma, a trend supported by the negative correlation of V/Sc with K_2O and SiO_2 in magmatic rocks of the CAOB (Fig. 6). This is consistent with the observation from South America by Halley (2020), who attributes the descending V/Sc ratios with decreasing Sc and increasing SiO_2 to the fractional crystallization of magnetite, given that the ion V^{4+} has a stronger affinity for magnetite than Sc^{3+} in oxidized magmas. Therefore, it is interpreted that it is high K_2O and SiO_2 in magma of porphyry Mo deposits rather than extremely low water content that account for the low V/Sc ratios in porphyry Mo deposits. In fact, the parental magmas in porphyry Mo deposits have high water contents (Audétat & Li, 2017; Shu *et al.*, 2019), which is also supported by high zircon Eu/Eu* (>0·3) of porphyry Mo deposits (Lu *et al.*, 2016). In the Junggar region of the western CAOB, geochemical data have shed light on the regional evolution from a juvenile oceanic arc composition characterized by low SiO_2, K_2O and Rb, and high MgO contents towards continental crust composition characterized by high SiO_2, K_2O and Rb, and low MgO contents (Tang *et al.*, 2019). Therefore, the gradual decrease of V/Sc ratios of magmatic rocks through time may have indicated the gradual evolution of crust in CAOB.

The control by the evolutionary process of crust on end members of porphyry-type systems in the CAOB is supported by elevated crustal residence age of porphyry Mo deposits relative to porphyry Cu ± Au ± Mo deposits (Fig. 7). The residence time (T_{Res}), also called crustal incubation time (Wang *et al.*, 2011), is the time difference between primitive crust formation dated by Nd-depleted-mantle model age and the crystallization age. The T_{Res} could serve as an ideal index for the crustal evolutionary processes in juvenile-material-dominated Central Asian Orogenic Belt, namely, how long the materials have existed since being extracted from

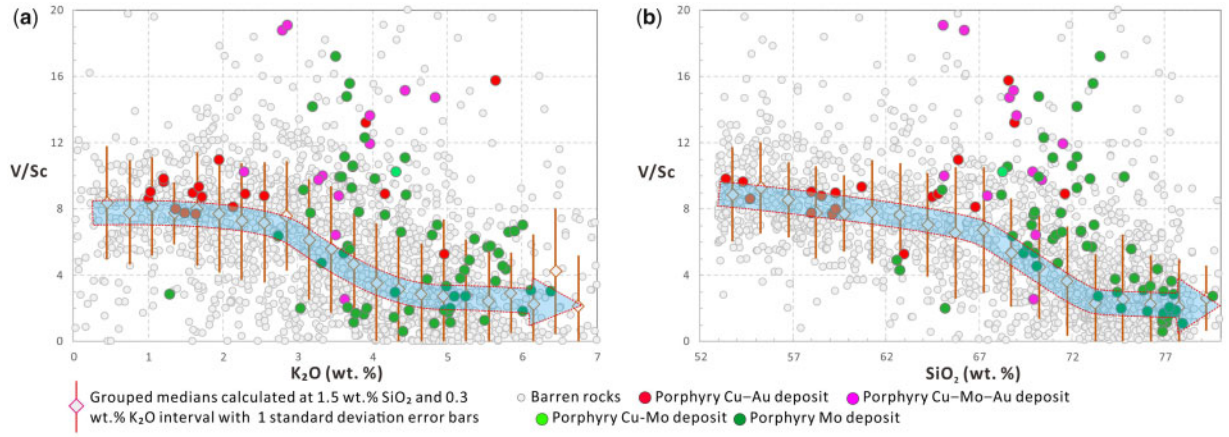

Fig. 6. Binary plots for (a) whole-rock V/Sc vs K_2O and (b) V/Sc vs SiO_2 of the igneous rocks in the CAOB. Grouped mediums are calculated at intervals of 1·5 wt % for SiO_2 and 0·3 wt % K_2O, respectively. Note that grouped medians for all data show the negative correlation of V/Sc with K_2O and SiO_2, highlighted by the transparent arrows. Porphyry Cu deposits are mainly distributed above the trend arrows, in contrast to porphyry Mo deposits having much wider V/Sc range.

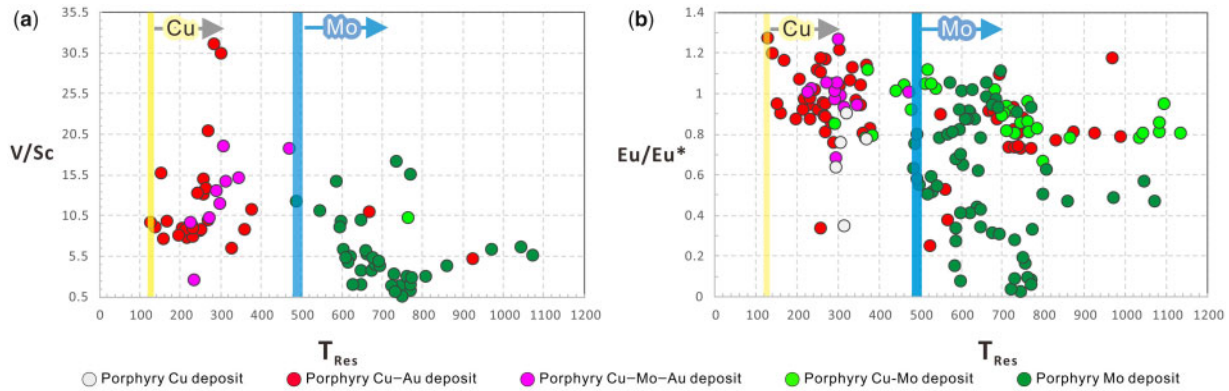

Fig. 7. Binary plots for crustal residence age (T_{Res}, Ma) from whole-rock Nd isotopes vs whole-rock V/Sc (a) and whole-rock Eu/Eu* (b) for porphyry Cu and Mo deposits in the CAOB. Note the T_{Res} for porphyry Mo deposits above 500 Ma and porphyry Cu deposits above 130 Ma, respectively.

the mantle before forming analysed igneous rocks. The T_{Res} of porphyry Cu deposits is mainly below 500 Ma in contrast to the porphyry Mo deposits generally above 500 Ma (Fig. 7), a trend consistent with the observed higher epsilon Nd and Hf values of porphyry Cu deposits relative to porphyry Mo deposits in the CAOB (Gao *et al.*, 2018). The T_{Res} of 500 Ma may represent the lower limit of the time interval for crustal material experiencing the evolution from the extraction of the mantle to the collisional event. Therefore, it is proposed T_{Res} of 500 Ma as the threshold to distinguish between porphyry Cu and Mo mineralization in the CAOB. Moreover, the T_{Res} for the ore-forming intrusions of porphyry Cu deposits is generally greater than 130 Ma (Fig. 7), which might be considered the lower limit for the residence age of porphyry Cu deposits, much shorter than that of the porphyry Mo deposits (T_{Res} lower limit of *c.*500 Ma) in the CAOB. Above observations of the formation of porphyry Cu deposits in more primitive crust in contrast to porphyry Mo deposit in the more evolved crust in CAOB are consistent with the distribution of Cu and Mo mineralized intrusive suites in eastern Australia (Blevin *et al.*, 1996) and Tibet (Hou *et al.*, 2015). Furthermore, it is also consistent with earlier work by Thompson et al. (1999), who proposed that Cu–Au mineralization is associated with chemically primary magmas, whereas Sn and Mo-rich deposits are associated with highly evolved magmas experiencing advanced fractional crystallization (Thompson *et al.*, 1999).

The crustal evolution could be constrained by crustal residence age, i.e. as immature crust evolves to mature state, the crustal thickness gradually increases, accompanied by increasing crustal residence age, which suggests the decrease of the proportion of juvenile material (Chiaradia, 2015). Such process is interpreted to control the transition of mineralization types from Cu–Au to Cu–Mo end-members. As crust thickens, the enhanced sulfide cumulate will sequester more Au than Cu from the parental magma if the cumulus sulfide is characterized by immiscible sulfide liquid rather than monosulfide solid solution when sulfide saturation is attained at high temperature and low pressure (Richards, 2009; Li & Audétat, 2013; Rottier *et al.*, 2019), which could

explain the preferential occurrence of Cu–Au in thin crust. Another explanation may be that magma emplacement in shallow crust may be optimized for high gold precipitation efficiency, which is supported by the Monte Carlo simulations for typical Au-rich porphyry Cu deposits (Chiaradia, 2020). Alternatively, tectonic regime (contraction vs. extension) could also control the formation of porphyry Cu–Mo and Cu–Au deposits in subduction zone. For example, in central Andes, the contractional events related to flattening of subducted slabs in southern Peru, northern and central Chile trigger crustal thickening and the formation of Cenozoic porphyry Cu–Mo (Skewes & Stern, 1994; Kay *et al.*, 1999; Perelló *et al.*, 2012), while the porphyry Cu–Au deposits in the Maricunga-El Indio belt are generated where coeval volcanism was active, implying more extensional tectonic conditions than Cu–Mo deposits (Kay *et al.*, 1994; Sillitoe, 2000; Sillitoe & Perelló, 2005). Such trends are interpreted to result from thin crust in extensional regime favouring porphyry Cu–Au deposits emplacing at shallow crustal depths, in contrast to thick crust in contractional regime favouring porphyry Cu–Mo deposits emplacing at deep crustal depths (Murakami *et al.*, 2010). In subsequent magmatic-hydrothermal process, Au is precipitated at a high rate since fluids exsolved from these shallow-level magmas, while Cu and Mo are precipitated at greater confining pressure at deep crustal depths (Murakami *et al.*, 2010; Chiaradia, 2020). Above interpretations are consistent with the general evolutionary history of crust, because a long-term and large-scale secular transition process is required for transforming primary thin oceanic arcs to evolved thick continental crust, which reinforces that crustal evolution controls the end-members of porphyry-type deposits.

Influence of crustal properties on porphyry deposits

Zircon is a robust and refractory mineral that can survive multiple recycling events, and incorporate U, Th and Hf but exclude Pb in its crystal structure, making it an important archive to record juvenile magma addition and crustal reworking during geodynamic evolution (Collins *et al.*, 2011; Spencer *et al.*, 2014; Dhuime *et al.*, 2017). Therefore, zircon Hf isotopes are ideal for clarifying the influence of crustal history on porphyry-type deposits. The zircon epsilon Hf values from the Paleozoic to Mesozoic together with the changing whole-rock La/Yb ratios (possibly a crude proxy for crustal thickness) are constructed for the western (Fig. 8a, c) and eastern (Fig. 8b, d) CAOB, respectively.

The western segment of CAOB In the western CAOB, the zircon εHf(t) values from the Cambrian to Silurian (*c.*540–420 Ma) have a wide range of *c.*-15 to +15 (Fig. 8a), suggesting magma derivation from both juvenile and ancient sources (Sun *et al.*, 2009). However, the minimum εHf(t) progressively increased from the Devonian to the Late Carboniferous (420–300 Ma), indicating that the crustal composition became increasingly juvenile, typical in extensional accretionary orogen (Kemp *et al.*, 2009). At *c.*300 Ma, εHf(t) shifted to negative values of *c.*-10, indicating continental collision (Smits *et al.*, 2014), which is consistent with the closure of the west segment of South Tianshan Ocean at the end of Late Carboniferous (Fig. 8a), a conclusion derived from the age of granite dike crosscutting the high pressure–low temperature Chinese South Tianshan metamorphic belt, the microfossils from the ophiolitic mélanges, and the stitching granitic plutons in the suture zone (Gao *et al.*, 2011; Han *et al.*, 2011). From *c.*300 to 250 Ma in eastern CAOB, the εHf(t) exhibited a converging trend with downward and upward shift of maximum and minimum values, respectively, which is similar to those of Paleoproterozoic magmatism in North Australian Craton (Iaccheri *et al.*, 2018) and Paleozoic magmatism in peri-Laurentia (Henderson *et al.*, 2018), indicating decreased reworking of ancient crust and homogenizing during post-collisional stage (Henderson *et al.*, 2018; Iaccheri *et al.*, 2018). There is another shift of εHf(t) to *c.*-10 at *c.*250 Ma, indicating collision with another continent (Smits *et al.*, 2014).

The two εHf(t) shifts at *c.*300 Ma and 250 Ma can shed new light on the existing debate on the final closure time of PAO in the western CAOB, i.e. the Late Carboniferous (Gao *et al.*, 2009; Han *et al.*, 2011) or the Late Permian to Middle Triassic (Xiao *et al.*, 2009a; Xiao *et al.*, 2015). According to this study, the shift of εHf(t) at *c.*300 Ma is represented by samples from the Chinese Altay–East Junggar collage and Tianshan range, while the shift at *c.*250 Ma is recorded by samples from the Tianshan range adjacent to the northern margin of the Tarim craton (Fig. 2). Moreover, the notable convergence of εHf(t) commencing at *c.*300 Ma in western CAOB (Fig. 8a) indicates the gradual homogenization of crust by reworking since the Late Carboniferous. Nonetheless, the crustal thickness continued to increase after the Late Carboniferous until the Late Permian at an average rate of *c.*0·3 km/Ma (Fig. 8c), indicating the amalgamation of the Tarim craton and the southern margin of CAOB. Therefore, it is proposed that closure of the branch of the western PAO, such as the west segment of the South Tianshan Ocean, occurred in the Late Carboniferous and shaped the fundamental architecture of the crust. However, the final closure of the western branch of PAO occurred at the boundary of Permian and Triassic, when the Tarim craton collided with the South margin of CAOB, resulting in the peak of crustal thickness at *c.*250 Ma (Fig. 8c). Such interpretation is supported by the reported evidences for the Triassic termination of final amalgamation of western CAOB, namely, the closure of east segment of South Tianshan Ocean and North Tianshan Ocean, including Permian ophiolites (Song *et al.*, 2015), the newly-recognized North Tianshan intra-oceanic arc amalgamated with the Yili–Central Tianshan arc by the Middle-Late Triassic as revealed by the change of detrital zircon province (Bai *et al.*, 2020), the Kangurtag suture zone

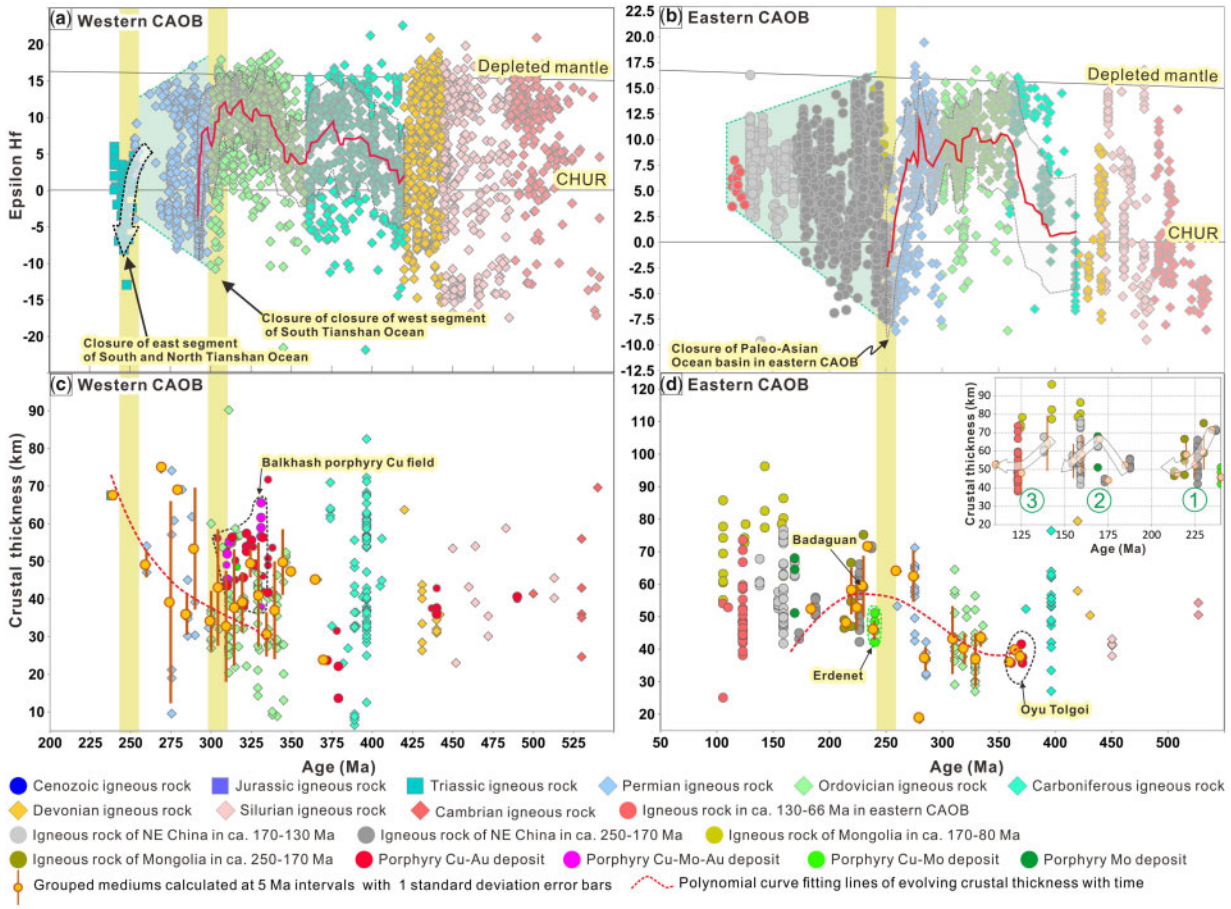

Fig. 8. Zircon epsilon Hf vs crystallizing age from igneous rocks in (a) western CAOB and (b) eastern CAOB; crustal thickness vs age of igneous rocks in (c) western CAOB and (d) eastern CAOB. Note that only one pulse of porphyry Mo mineralization is present in (d) after filtering of crustal thickness proxy. The inset in (d) illustrates the varying crustal thickness in eastern CAOB during the Mesozoic. The thicknesses of crust were calculated by La/Yb ratios of each sample (Profeta *et al.*, 2015), using the same filter criteria as in Profeta *et al.* (2015), with details listed in Supplementary Data Document. The red solid line in the middle of the two transparent fields in (a) and (b) are the moving averages with the fields denoting standard deviations. Grouped medians are calculated at intervals of 5 Ma for age. In Western CAOB, the increasing crustal thickness from the Carboniferous to Permian roughly described in an average rate of *c.*0·3 km/Ma (c), is accompanied by the decreasing epsilon Hf values, suggesting the gradual evolving process from thin juvenile to thick ancient crust. In Eastern CAOB, the abrupt shift of εHf(t) values at *c.*250 Ma (b) is coupled with a peak for crustal thickness (d), which marks the closure of eastern Paleo-Asian Ocean.

recording the final closure of the North Tianshan Ocean via two-way subduction suggested by the mélange and detrital zircons in turbiditic sandstones (Chen *et al.*, 2019). Also worth noting are coupled decreases in εHf(t) values (Fig. 8a) and crustal thickness (Fig. 8c) during the 380–350 Ma, suggesting the mixture between mantle-derived magma and old continental crust under extensional setting induced by subduction initiation of the South Tianshan Ocean (Han *et al.*, 2015; Bao *et al.*, 2018).

The porphyry Cu ± Au ± Mo deposits that formed in the Early Paleozoic were emplaced in thinner crust (generally < 40 km) of island arcs relative to those formed in the crust generally thicker than 40 km during the Late Paleozoic in Balkhash region, the most significant porphyry Cu field in western CAOB (Fig. 8c). The Late Paleozoic metallogenic event clusters into *c.*330–300 Ma approaching the closure of the north branch of PAO. Such a period is interpreted as one of the four Phanerozoic global high magmatic addition rates (MARs), during which the island and continental arcs in several unrelated regions worldwide synchronously produced higher volumes of magma (> 1000 km^2/Ma) than normal (Ducea *et al.*, 2015). The MARs peak of the CAOB is in the Carboniferous, speculated to be linked to global accelerated production of the juvenile crust (Ducea *et al.*, 2015), which favors forming large-sized magma chambers and hydrous ore-forming magmas in magmatic arcs (Zhang & Audétat, 2017), thus might account for the massive formation of porphyry Cu deposits in the Balkhash region during the Carboniferous. Besides, the conspicuous link of porphyry Mo deposits to post-subduction setting suggests that the crustal reworking may favour the formation of large-sized and long-lived magma chamber, and consequent emplacement of mineralization intrusions in deep level characterized by slow rates of crystallization, all of which are considered as the favourable controlling factor on

forming porphyry Mo deposits (Audétat & Li, 2017; Shinohara *et al.*, 1995).

The eastern segment of CAOB The εHf(t) at 400–250 Ma displays an inverted 'U-shaped' array, which is remarkably similar to that of 1700–1200 Ma magmatism in central Australia (Smits *et al.*, 2014), reflecting the transition from a continental arc to an extensional, accretionary orogen, followed by terminal continental collision (Fig. 8b). The shift of εHf(t) from negative to positive values at 400–370 Ma suggests the transition of crustal reservoir from ancient (represented by negative εHf(t) values) to juvenile (represented by positive εHf(t) values) compositions via the massive addition of juvenile materials such as in arcs (Sun *et al.*, 2009). In accordance with the progressive rejuvenation of crust during *c.*400–370 Ma, the Oyu Tolgoi porphyry deposit, the largest Cu–Au deposit in the CAOB, was formed in the Gurvansayhan island arc dominated by juvenile materials in South Mongolia (Shen *et al.*, 2018). Conversely, the notable shift of εHf(t) from positive to the negative values at c. 270–250 Ma suggests the transition of juvenile to ancient crustal composition through the massive addition of old/reworked material due to collision, consistent with the generally accepted closure time of the Paleo-Asian Ocean basin in the eastern CAOB (Wu *et al.*, 2011). This is in accordance with the accepted interpretation of final closure of PAO in eastern CAOB at the Permian–Triassic (Xiao *et al.*, 2015), which is supported by the geological evidences such as Late Carboniferous to the Middle Permian Andean-type active magmatic arc (Zhang et al., 2009), Permian cherts (Xie *et al.*, 2014), the Permian deformed and recrystallized granitic–granodioritic porphyries (Lin *et al.*, 2014), blueschists with Triassic protolith ages (Chu *et al.*, 2013), and Triassic syn-collisional crust-derived granite (Li *et al.*, 2007). A similar pattern has also been reported in the Tibetan orogen, where the magmatic zircon grains show depleted mantle-type positive εHf(t) throughout the Mesozoic but shift markedly to negative values at *c.*55 Ma, a trend recording the subduction of Himalayan sediment to the southern Lhasa terrane driven by India–Asia collision(Chu *et al.*, 2011).

The long-lasting debate on the contrasting roles of juvenile and reworked materials in the crustal generation in the eastern CAOB can be clarified by the notable convergence of εHf(t) during the Mesozoic as highlighted by the pale green trapezoid in Figure 8b. Similar to the converging trend at 300–250 Ma in western CAOB, such εHf(t) array is interpreted to record the homogenization of crust by the mixture between the ancient and juvenile crustal materials, accompanied by the progressive destruction of existing ancient crustal materials during crustal reworking (Collins *et al.*, 2011). It further reveals that no significant injection of juvenile material to the evolving crust during the Mesozoic, a process otherwise would inevitably increase εHf(t) to values close to the evolutionary line of the depleted mantle (Fig. 8b). Given that the collected Hf isotopic data generally covered the eastern CAOB, it's therefore concluded that the fundamental architecture and compositions of the crust beneath the eastern segment of CAOB had been completed by *c.*250 Ma, marked by the closure of Paleo-Asian Ocean, while the overprints of the Mongol–Okhotsk Ocean and Paleo-Pacific Ocean regimes predominantly reworked the existing juvenile crustal materials. In general, after the closure of Paleo-Asian Ocean along the Solonker suture zone in eastern CAOB at *c.* 250 Ma, magma resources from the Middle Triassic to the Cenozoic experienced gradual mixing between the juvenile and ancient crustal materials via reworking the crust formed in previous subduction-accretion process. Similarly, after the closure of west Tianshan suture zone in western CAOB at *c.*300 Ma, the subduction-accretion process was terminated and magma resources from the Early Permian to the Triassic originate from gradual mingling of melt derived from the juvenile and ancient materials in the crust, as illustrated by the convergent of upper and lower limits of εHf(t) with decreasing age (Fig. 8a).

The crustal thickness in the eastern CAOB demonstrates a gradual increase commencing at *c.* 350 Ma, with the peak occurring at *c.*250 Ma (Fig. 8d), recording the collision between the eastern CAOB and the North China craton. The porphyry Cu–Au deposits were formed in thin crust (generally $<$ 40 km) of island arcs preceding the thickening event, while the porphyry Cu–Mo and Mo deposits were mainly formed in the thick crust (generally $>$ 40 km) after *c.*250 Ma. The porphyry Cu–Mo deposits (e.g. the Erdenet, Wunugetushan, Badaguan, and Taipingchuan Cu–Mo deposits) in the eastern CAOB were produced by the subduction of Mongol–Okhotsk Ocean in the Mesozoic (Gao *et al.*, 2018; Shen *et al.*, 2018), an interpretation reinforced by the increasing crustal thickness forming these Cu–Mo deposits (Fig. 8d), in keeping with the closure of the Mongol–Okhotsk Ocean in the Middle Jurassic (Wu *et al.*, 2011; Shu *et al.*, 2016; Chen *et al.*, 2017).

As outlined by the inset in Fig. 8d, the three pulses of porphyry Mo deposits in Northeast China are also tracked by the evolution of crustal thickness of eastern CAOB with time. The first pulse was related to extension following the collision between eastern CAOB and North China craton (Shu *et al.*, 2016), supported by the decreasing crustal thickness during the Triassic (*c.*250–200 Ma). The debate on the triggers for the second pulse in the Jurassic, i.e. the flat-slab subduction of the Paleo-Pacific plate (Shu *et al.*, 2016) or the consumption of the Mongol–Okhotsk Ocean (Chen *et al.*, 2017), may also be resolved because the crust thickness gradually increases during the Early to Middle Jurassic (*c.*200–160 Ma) then decreases during the Middle to Late Jurassic (*c.*160–140 Ma; seeing the inset in Figure 8d), consistent with the subduction and post-subduction of the Mongol–Okhotsk Ocean (Chen *et al.*, 2017). The third pulse was formed by the lithospheric thinning resulted from slab rollback of the Paleo-Pacific Ocean,

generally consistent with the decreasing crustal thickness during the Cretaceous (Shu *et al.*, 2016; Chen *et al.*, 2017).

CONCLUSIONS

The distinctly higher zircon Eu/Eu* and whole-rock V/Sc ratios of the ore-forming porphyries for Cu ± Au ± Mo deposits compared to ore-barren igneous rocks, suggest the control by dissolved water content in magma on mineralizing potential, which is further quantified by an empirical formula of the V/Sc ratios and Cu tonnages of porphyry Cu deposits. The high water contents of parental magma may reflect magma chambers in the upper crust supplying large amounts of water and metals to promote the tonnages of porphyry Cu deposits.

The generally decreasing V/Sc from the Paleozoic to Mesozoic in the CAOB indicates the gradual evolution of crust from the juvenile oceanic arc to continental crust, favorable for forming porphyry Cu and Mo deposits, respectively. The crustal residence age (T_{Res}) of *c.*500 Ma is proposed as the threshold distinguishing porphyry Cu and Mo deposits in the CAOB, with the T_{Res} above 500 Ma favoring porphyry Mo mineralization, which could be applied to assess whether a certain target region is favorable for porphyry Cu or Mo mineralization.

The basic architecture of crust in the western and eastern CAOB had been built by *c.*300 Ma and *c.*250 Ma, respectively, with the subsequent geological evolution solely reworking and homogenizing the juvenile crust. In the eastern segment, porphyry Cu ± Au ± Mo deposits originated from juvenile materials in thin island arcs, while porphyry Mo deposits were formed by reworked materials in the thickened orogenic crust after c. 250 Ma. In the western segment, porphyry Cu ± Mo ± Au deposits in the Balkhash region were formed in the thickened continental crust (generally $>$ 40 km) during the Late Carboniferous, in contrast to the porphyry Cu ± Au deposits formed in thin island arc (generally $<$ 40 km) during the Early Paleozoic.

ACKNOWLEDGMENTS

We acknowledge Christopher Spencer, Robert Loucks and Wenjiao Xiao for their thorough reviews of this manuscript. We also thank Andreas Audétat for the handling of this manuscript. This is contribution 1612 from the ARC Centre of Excellence for Core to Crust Fluid Systems (http://www.CCFS.mq.edu.au). YL publishes with permission of the Executive Director, Geological Survey of Western Australia. This is contribution No.IS-2989 from GIGCAS.

FUNDING

This study was financially supported by the Chinese National Science Fund for Distinguished Young Scholars (41725009) and Type-B Chinese Academy of Sciences Strategic Pilot Science and Technology Special (XDB18030206).

SUPPLEMENTARY DATA

Supplementary data are available at *Journal of Petrology* online.

REFERENCES

Annen, C., Blundy, J. D. & Sparks, R. S. J. (2006). The genesis of intermediate and silicic magmas in deep crustal hot zones. *Journal of Petrology* **47**, 505–539.

Audétat, A. & Li, W. T. (2017). The genesis of Climax-type porphyry Mo deposits: Insights from fluid inclusions and melt inclusions. *Ore Geology Reviews* **88**, 436–460.

Bai, X. Y., Chen, Y. H., Song, D. F., Xiao, W. J., Windley, B. F., Ao, S. J., Li, L. & Xiang, D. F. (2020). A new Carboniferous-Permian intra-oceanic subduction system in the North Tianshan (NW China): Implications for multiple accretionary tectonics of the southern Altaids. *Geological Journal* **55**, 2232–2253.

Bao, Z. H., Cai, K. D., Sun, M., Xiao, W. J., Wan, B., Wang, Y. N., Wang, X. S. & Xia, X. P. (2018). Continental crust melting induced by subduction initiation of the South Tianshan Ocean: Insight from the Latest Devonian granitic magmatism in the southern Yili Block. *Journal of Asian Earth Sciences* **153**, 100–117.

Blevin, P. L., Chappell, B. W. & Allen, C. M. (1996). Intrusive metallogenic provinces in eastern Australia based on granite source and composition. *Earth and Environmental Science Transactions of the Royal Society of Edinburgh* **87**, 281–290.

Candela, P. A. & Piccoli, P. M. (2005). Magmatic processes in the development of porphyry-type ore systems. *Economic Geology 100th Anniversary Volume* **100**, 25–38.

Cawthorn, R. G. (1976). Melting relations in part of the system CaO-MgO-Al_2O_3-SiO_2-Na_2O-H_2O under 5kb pressure. *Journal of Petrology* **17**, 44–72.

Černy, P., Blevin, P. L., Cuney, M. & London, D. (2005). Granite-related ore deposits. *Economic Geology 100th Anniversary Volume* **100**, 337–370.

Chen, H. Y. & Wu, C. (2020). Metallogenesis and major challenges of porphyry copper systems above subduction zones. *Science China Earth Sciences* **63**, 899–918.

Chen, Y. J., Zhang, C., Wang, P., Pirajno, F. & Li, N. (2017). The Mo deposits of Northeast China: A powerful indicator of tectonic settings and associated evolutionary trends. *Ore Geology Reviews* **81**, 602–640.

Chen, Z. Y., Xiao, W. J., Windley, B. F., Schulmann, K., Mao, Q. G., Zhang, Z. Y., Zhang, J., Deng, C. & Song, S. H. (2019). Composition, provenance, and tectonic setting of the southern Kangurtag accretionary complex in the eastern Tianshan, NW China: Implications for the Late Paleozoic evolution of the North Tianshan Ocean. *Tectonics* **38**, 2779–2802.

Chiaradia, M. (2014). Copper enrichment in arc magmas controlled by overriding plate thickness. *Nature Geoscience* **7**, 43–46.

Chiaradia, M. (2015). Crustal thickness control on Sr/Y signatures of recent arc magmas: an Earth scale perspective. *Scientific Reports* **5**, 8115.

Chiaradia, M. (2020). Gold endowments of porphyry deposits controlled by precipitation efficiency. *Nature Communications* **11**,

Chu, H., Zhang, J. R., Wei, C. J., Wang, H. C. & Ren, Y. W. (2013). A new interpretation of the tectonic setting and age of

meta-basic volcanics in the Ondor Sum Group, Inner Mongolia. *Chinese Science Bulletin* **58**, 3580–3587.

Chu, M. F., Chung, S. L., O'Reilly, S. Y., Pearson, N. J., Wu, F. Y., Li, X. H., Liu, D. y., Ji, J. Q., Chu, C. H. & Lee, H. Y. (2011). India's hidden inputs to Tibetan orogeny revealed by Hf isotopes of Transhimalayan zircons and host rocks. *Earth and Planetary Science Letters* **307**, 479–486.

Collins, W. J., Belousova, E. A., Kemp, A. I. S. & Murphy, J. B. (2011). Two contrasting Phanerozoic orogenic systems revealed by hafnium isotope data. *Nature Geoscience* **4**, 333–337.

Cooke, D. R., Hollings, P. & Walshe, J. L. (2005). Giant porphyry deposits: characteristics, distribution, and tectonic controls. *Economic Geology* **100**, 801–818.

Dhuime, B., Hawkesworth, C. J., Delavault, H. & Cawood, P. A. (2017). Continental growth seen through the sedimentary record. *Sedimentary Geology* **357**, 16–32.

Du, J. G. & Audétat, A. (2020). Early sulfide saturation is not detrimental to porphyry Cu–Au formation. *Geology* **48**, 519–524.

Ducea, M. N., Paterson, S. R. & DeCelles, P. G. (2015). High-volume magmatic events in subduction systems. *Elements* **11**, 99–104.

Gao, J., Klemd, R., Qian, Q., Zhang, X., Li, J. L., Jiang, T. & Yang, Y. Q. (2011). The collision between the Yili and Tarim blocks of the Southwestern Altaids: Geochemical and age constraints of a leucogranite dike crosscutting the HP-LT metamorphic belt in the Chinese Tianshan Orogen. *Tectonophysics* **499**, 118–131.

Gao, J., Long, L. L., Klemd, R., Qian, Q., Liu, D. Y., Xiong, X. M., Su, W., Liu, W., Wang, Y. T. & Yang, F. Q. (2009). Tectonic evolution of the South Tianshan orogen and adjacent regions, NW China: geochemical and age constraints of granitoid rocks. *International Journal of Earth Sciences* **98**, 1221–1238.

Gao, J., Qin, K. Z., Zhou, M. F. & Zaw, K. (2018). Large-scale porphyry-type mineralization in the Central Asian Metallogenic Domain: Geodynamic background, magmatism, fluid activity and metallogenesis. *Journal of Asian Earth Sciences* **165**, 1–6.

Geng, H. Y., Sun, M., Yuan, C., Xiao, W. J., Xian, W. S., Zhao, G. C., Zhang, L. F., Wong, K. & Wu, F. Y. (2009). Geochemical, Sr-Nd and zircon U–Pb-Hf isotopic studies of Late Carboniferous magmatism in the West Junggar, Xinjiang: Implications for ridge subduction? *Chemical Geology* **266**, 364–389.

Halley, S. (2020). Mapping magmatic and hydrothermal processes from routine exploration geochemical analyses. *Economic Geology* **115**, 489–503.

Halter, W. E., Heinrich, C. A. & Pettke, T. (2005). Magma evolution and the formation of porphyry Cu–Au ore fluids: evidence from silicate and sulfide melt inclusions. *Mineralium Deposita* **39**, 845–863.

Han, B. F., He, G. Q. & Wang, S. G. (1999). Postcollisional mantle-derived magmatism, underplating and implications for basement of the Junggar Basin. *Science in China Series D: Earth Sciences* **42**, 113–119.

Han, B. F., He, G. Q., Wang, X. C. & Guo, Z. J. (2011). Late Carboniferous collision between the Tarim and Kazakhstan-Yili terranes in the western segment of the South Tian Shan Orogen, Central Asia, and implications for the Northern Xinjiang, western China. *Earth-Science Reviews* **109**, 74–93.

Han, B. F., Ji, J. Q., Song, B., Chen, L. H. & Zhang, L. (2006). Late Paleozoic vertical growth of continental crust around the Junggar Basin, Xinjiang, China (Part I) : Timing of post-collisional plutonism. *Acta Petrologica Sinica* **22**, 1077–1086.

Han, Y. G., Zhao, G. C., Sun, M., Eizenhofer, P. R., Hou, W. Z., Zhang, X. R., Liu, D. X., Wang, B. & Zhang, G. W. (2015). Paleozoic accretionary orogenesis in the Paleo-Asian Ocean: Insights from detrital zircons from Silurian to Carboniferous strata at the northwestern margin of the Tarim Craton. *Tectonics* **34**, 334–351.

Hawkesworth, C., Cawood, P. A. & Dhuime, B. (2019). Rates of generation and growth of the continental crust. *Geoscience Frontiers* **10**, 165–173.

Henderson, B. J., Collins, W. J., Murphy, J. B. & Hand, M. (2018). A hafnium isotopic record of magmatic arcs and continental growth in the Iapetus Ocean: The contrasting evolution of Ganderia and the peri-Laurentian margin. *Gondwana Research* **58**, 141–160.

Hou, Z. Q., Duan, L. F., Lu, Y. J., Zheng, Y. C., Zhu, D. C., Yang, Z. M., Yang, Z. S., Wang, B. D., Pei, Y. R., Zhao, Z. D. & McCuaig, T. C. (2015). Lithospheric architecture of the Lhasa terrane and its control on ore deposits in the Himalayan-Tibetan orogen. *Economic Geology* **110**, 1541–1575.

Iaccheri, L. M., Kemp, A. I. S. & EIMF (2018). Detrital zircon age, oxygen and hafnium isotope systematics record rigid continents after 2.5 Ga. *Gondwana Research* **57**, 90–118.

Jahn, B. M. (2004). The Central Asian Orogenic Belt and growth of the continental crust in the Phanerozoic. *Geological Society, London, Special Publications* **226**, 73–100.

Jahn, B. M., Capdevila, R., Liu, D. Y., Vernon, A. & Badarch, G. (2004). Sources of Phanerozoic granitoids in the transect Bayanhongor-Ulaan Baatar, Mongolia: geochemical and Nd isotopic evidence, and implications for Phanerozoic crustal growth. *Journal of Asian Earth Sciences* **23**, 629–653.

Jahn, B. M., Wu, F. Y. & Chen, B. (2000). Granitoids of the Central Asian Orogenic Belt and continental growth in the Phanerozoic. *Geological Society of America Special Papers* **350**, 181–193.

James, G. B. (1981). *Orogenic Andesites and Plate Tectonics.* Berlin: Springer.

Jenner, F. E., O'neill, H. S. C., Arculus, R. J. & Mavrogenes, J. A. (2010). The magnetite crisis in the evolution of arc-related magmas and the initial concentration of Au, Ag and Cu. *Journal of Petrology* **51**, 2445–2464.

Jugo, P. J. (2009). Sulfur content at sulfide saturation in oxidized magmas. *Geology* **37**, 415–418.

Kay, S. M., Mpodozis, C. & Coira, B. (1999). Neogene magmatism, tectonics, and mineral deposits of the central Andes (22° to 33° S latitude). *Society of Economic Geologists Special Publication* **7**, 27–59.

Kay, S. M., Mpodozis, C., Tittler, A. & Cornejo, P. (1994). Tertiary magmatic evolution of the Maricunga mineral belt in Chile. *International Geology Review* **36**, 1079–1112.

Kemp, A. I. S., Hawkesworth, C. J., Collins, W. J., Gray, C. M. & Blevin, P. L, & EIMF (2009). Isotopic evidence for rapid continental growth in an extensional accretionary orogen: The Tasmanides, eastern Australia. *Earth and Planetary Science Letters* **284**, 455–466.

Lee, C. T. A., Lee, T. C. & Wu, C. T. (2014). Modeling the compositional evolution of recharging, evacuating, and fractionating (REFC) magma chambers: Implications for differentiation of arc magmas. *Geochimica et Cosmochimica Acta* **143**, 8–22.

Lee, C. T. A., Luffi, P., Chin, E. J., Bouchet, R., Dasgupta, R., Morton, D. M., Le Roux, V., Yin, Q. Z. & Jin, D. (2012). Copper systematics in arc magmas and implications for crust-mantle differentiation. *Science (New York, N.Y.)* **336**, 64–68.

Leeman, W. P. (2001). The influence of subduction zone thermal structure on arc magma chemistry: B and fluid-mobile elements. *AGU Fall Meeting Abstracts*.

Li, J. Y., Gao, L. M., Sun, G. H., Li, Y. P. & Wang, Y. B. (2007). Shuangjingzi middle Triassic syn-collisional crust-derived granite in the east Inner Mongolia and its constraint on the timing of collision between Siberian and Sino-Korean paleo-plates. *Acta Petrologica Sinica* **23**, 565–582.

Li, S., Wang, T., Wilde, S. A. & Tong, Y. (2013). Evolution, source and tectonic significance of Early Mesozoic granitoid magmatism in the Central Asian Orogenic Belt (central segment). *Earth-Science Reviews* **126**, 206–234.

Li, Y. & Audétat, A. (2013). Gold solubility and partitioning between sulfide liquid, monosulfide solid solution and hydrous mantle melts: Implications for the formation of Au-rich magmas and crust-mantle differentiation. *Geochimica et Cosmochimica Acta* **118**, 247–262.

Lin, L. N., Xiao, W. J., Wan, B., Windley, B. F., Ao, S. J., Han, C. M., Feng, J. Y., Zhang, J. E. & Zhang, Z. Y. (2014). Geochronologic and geochemical evidence for persistence of south-dipping subduction to Late Permian time, Langshan Area, Inner Mongolia (China). *American Journal of Science* **314**, 679–703.

Loader, M. A., Wilkinson, J. J. & Armstrong, R. N. (2017). The effect of titanite crystallisation on Eu and Ce anomalies in zircon and its implications for the assessment of porphyry Cu deposit fertility. *Earth and Planetary Science Letters* **472**, 107–119.

Long, L. L., Gao, J., Klemd, R., Beier, C., Qian, Q., Zhang, X., Wang, J. B. & Jiang, T. (2011). Geochemical and geochronological studies of granitoid rocks from the Western Tianshan Orogen: Implications for continental growth in the southwestern Central Asian Orogenic Belt. *Lithos* **126**, 321–340.

Loucks, R. R. (2014). Distinctive composition of copper-ore--forming arcmagmas. *Australian Journal of Earth Sciences* **61**, 5–16.

Loucks, R. R., Fiorentini, M. L. & Henríquez, G. J. (2020). New magmatic oxybarometer using trace elements in zircon. *Journal of Petrology* **61**,

Lu, Y. J., Loucks, R. R., Fiorentini, M. L., McCuaig, T. C., Evans, N. J., Yang, Z. M., Hou, Z. Q., Kirkland, C. L., Parra-Avila, L. A. & Kobussen, A. (2016). Zircon compositions as a pathfinder for porphyry Cu ± Mo ± Au mineral deposits. *Society of Economic Geologists Special Publication* **19**, 319–347.

Lu, Y. J., Loucks, R. R., Fiorentini, M. L., Yang, Z. M. & Hou, Z. Q. (2015). Fluid flux melting generated postcollisional high Sr/Y copper ore-forming water-rich magmas in Tibet. *Geology* **43**, 583–586.

Lu, Y. J., Smithies, R. H., Wingate, M. T. D., Evans, N. J., McCuaig, T. C., Champion, D. C. & Outhwaite, M. (2019). Zircon fingerprinting of magmatic-hydrothermal systems in the Archean Yilgarn craton. *Perth: Geological Survey of Western Australia* **22**,

Matjuschkin, V., Blundy, J. D. & Brooker, R. A. (2016). The effect of pressure on sulphur speciation in mid-to deep-crustal arc magmas and implications for the formation of porphyry copper deposits. *Contributions to Mineralogy and Petrology* **171**,

Mazukabzov, A. M., Donskaya, T. V., Gladkochub, D. P. & Paderin, I. P. (2010). The Late Paleozoic geodynamics of the West Transbaikalian segment of the Central Asian fold belt. *Russian Geology and Geophysics* **51**, 482–491.

Middlemost, E. A. K. (1994). Naming materials in the magma/igneous rock system. *Earth-Science Reviews* **37**, 215–224.

Mungall, J. E. (2002). Roasting the mantle: Slab melting and the genesis of major Au and Au-rich Cu deposits. *Geology* **30**, 915–918.

Murakami, H., Seo, J. H. & Heinrich, C. A. (2010). The relation between Cu/Au ratio and formation depth of porphyry-style Cu–Au ± Mo deposits. *Mineralium Deposita* **45**, 11–21.

Perelló, J., Sillitoe, R., Mpodozis, C., Brockway, H. & Posso, H. (2012). Geologic setting and evolution of the porphyry copper-molybdenum and copper-gold deposits at Los Pelambres, central Chile. *Society of Economic Geologists* **16**, 79–104.

Plank, T., Kelley, K. A., Zimmer, M. M., Hauri, E. H. & Wallace, P. J. (2013). Why do mafic arc magmas contain similar to 4 wt% water on average? *Earth and Planetary Science Letters* **364**, 168–179.

Profeta, L., Ducea, M. N., Chapman, J. B., Paterson, S. R., Gonzales, S. M., Kirsch, M., Petrescu, L. & Decelles, P. G. (2015). Quantifying crustal thickness over time in magmatic arcs. *Scientific Reports* **5**, 17786.

Richards, J. P. (2003). Tectono-magmatic precursors for porphyry Cu-(Mo-Au) deposit formation. *Economic Geology* **98**, 1515–1533.

Richards, J. P. (2009). Postsubduction porphyry Cu–Au and epithermal Au deposits: Products of remelting of subduction--modified lithosphere. *Geology* **37**, 247–250.

Richards, J. P. (2011). High Sr/Y arc magmas and porphyry Cu ± Mo ± Au deposits: just add water. *Economic Geology* **106**, 1075–1081.

Richards, J. P., Spell, T., Rameh, E., Razique, A. & Fletcher, T. (2012). High Sr/Y magmas reflect arc maturity, high magmatic water content, and porphyry Cu±Mo±Au potential: Examples from the Tethyan arcs of central and eastern Iran and western Pakistan. *Economic Geology* **107**, 295–332.

Rohrlach, B. & Loucks, R. (2005). Multi-million-year cyclic ramp-up of volatiles in a lower crustal magma reservoir trapped below the Tampakan copper-gold deposit by Mio-Pliocene crustal compression in the southern Philippines. In: Porter, T.M. (ed.), *Super Porphyry Copper & Gold Deposits—A Global Perspective*. Adelaide: PCG Publishing, pp. 369–407.

Rottier, B., Audétat, A., Koděra, P. & Lexa, J. (2019). Origin and Evolution of Magmas in the Porphyry Au-mineralized Javorie Volcano (Central Slovakia): Evidence from Thermobarometry, Melt Inclusions and Sulfide Inclusions. *Journal of Petrology* **60**, 2449–2482.

Seedorff, E., Dilles, J. H., Proffett, J. M., Einaudi, M. T., Zurcher, L., Stavast, W. J. A., Johnson, D. A. & Barton, M. D. (2005). Porphyry deposits: Characteristics and origin of hypogene features. *Economic Geology 100th Anniversary Volume* **29**, 251–298.

Seltmann, R., Porter, T. M. & Pirajno, F. (2014). Geodynamics and metallogeny of the central Eurasian porphyry and related epithermal mineral systems: a review. *Journal of Asian Earth Sciences* **79**, 810–841.

Sengör, A. M. C., Natal'in, B. A. & Burtman, V. S. (1993). Evolution of the Altaid tectonic collage and Paleozoic crustal growth in Eurasia. *Nature* **364**, 299–307.

Shen, P., Pan, H., Hattori, K., Cooke, D. R. & Seitmuratova, E. (2018). Large Paleozoic and Mesozoic porphyry deposits in the Central Asian Orogenic Belt: Geodynamic settings, magmatic sources, and genetic models. *Gondwana Research* **58**, 161–194.

Shinohara, H., Kazahaya, K. & Lowenstern, J. B. (1995). Volatile transport in a convecting magma column: Implications for porphyry Mo mineralization. *Geology* **23**, 1091–1094.

Shu, Q. H., Chang, Z. S., Lai, Y., Hu, X. L., Wu, H. Y., Zhang, Y., Wang, P., Zhai, D. G. & Zhang, C. (2019). Zircon trace elements and magma fertility: insights from porphyry (-skarn) Mo deposits in NE China. *Mineralium Deposita* **54**, 645–656.

Shu, Q. H., Chang, Z. S., Lai, Y., Zhou, Y. T., Sun, Y. & Yan, C. (2016). Regional metallogeny of Mo-bearing deposits in northeastern China, with new Re–Os dates of porphyry Mo

deposits in the northern Xilamulun district. *Economic Geology* **111**, 1783–1798.

Sillitoe, R. H. (2000). Gold-rich porphyry deposits: descriptive and genetic models and their role in exploration and discovery. *Reviews in Economic Geology* **13**, 315–345.

Sillitoe, R. H. (2010). Porphyry copper systems. *Economic Geology* **105**, 3–41.

Sillitoe, R. H. & Perelló, J. (2005). Andean copper province: Tectonomagmatic settings, deposit types, metallogeny, exploration, and discovery. *Economic Geology 100th Anniversary Volume* 845–890.

Skewes, M. A. & Stern, C. R. (1994). Tectonic trigger for the formation of Late Miocene Cu-rich breccia pipes in the Andes of Central Chile. *Geology* **22**, 551–554.

Smits, R. G., Collins, W. J., Hand, M., Dutch, R. & Payne, J. (2014). A Proterozoic Wilson cycle identified by Hf isotopes in central Australia: Implications for the assembly of Proterozoic Australia and Rodinia. *Geology* **42**, 231–234.

Song, S. G., Wang, M. M., Xu, X., Wang, C., Niu, Y. L., Allen, M. B. & Su, L. (2015). Ophiolites in the Xing'an-Inner Mongolia accretionary belt of the CAOB: Implications for two cycles of seafloor spreading and accretionary orogenic events. *Tectonics* **34**, 2221–2248.

Spencer, C. J., Cawood, P. A., Hawkesworth, C. J., Raub, T. D., Prave, A. R. & Roberts, N. M. W. (2014). Proterozoic onset of crustal reworking and collisional tectonics: Reappraisal of the zircon oxygen isotope record. *Geology* **42**, 451–454.

Spencer, C. J., Dyck, B., Mottram, C. M., Roberts, N. M. W., Yao, W. H. & Martin, E. L. (2019). Deconvolving the pre-Himalayan Indian margin - Tales of crustal growth and destruction. *Geoscience Frontiers* **10**, 863–872.

Sun, M., Long, X. P., Cai, K. D., Jiang, Y. D., Wang, B. Y., Yuan, C., Zhao, G. C., Xiao, W. J. & Wu, F. Y. (2009). Early Paleozoic ridge subduction in the Chinese Altai: Insight from the abrupt change in zircon Hf isotopic compositions. *Science in China Series D: Earth Sciences* **52**, 1345–1348.

Tang, G. J., Wang, Q., Wyman, D. A. & Dan, W. (2019). Crustal maturation through chemical weathering and crustal recycling revealed by Hf-O-B isotopes. *Earth and Planetary Science Letters* **524**, 115709–115708.

Thompson, J. F. H., Sillitoe, R. H., Baker, T., Lang, J. R. & Mortensen, J. K. (1999). Intrusion related gold deposits associated with tungsten-tin provinces. *Mineralium Deposita* **34**, 323–334.

Tong, Y., Jahn, B. M., Wang, T., Hong, D. W., Smith, E. I., Sun, M., Gao, J. F., Yang, Q. D. & Huang, W. (2015). Permian alkaline granites in the Erenhot-Hegenshan belt, northern Inner Mongolia, China: Model of generation, time of emplacement and regional tectonic significance. *Journal of Asian Earth Sciences* **97**, 320–336.

Wang, C. Y., Campbell, I. H., Stepanov, A. S., Allen, C. M. & Burtsev, I. N. (2011). Growth rate of the preserved continental crust: II. Constraints from Hf and O isotopes in detrital zircons from Greater Russian Rivers. *Geochimica et Cosmochimica Acta* **75**, 1308–1345.

Wang, T., Tong, Y., Zhang, L., Li, S., Huang, H., Zhang, J. J., Guo, L., Yang, Q. D., Hong, D. W., Donskaya, T., Gladkochub, D. & Tserendash, N. (2017). Phanerozoic granitoids in the central and eastern parts of Central Asia and their tectonic significance. *Journal of Asian Earth Sciences* **145**, 368–392.

Wilhem, C., Windley, B. F. & Stampfli, G. M. (2012). The Altaids of Central Asia: A tectonic and evolutionary innovative review. *Earth-Science Reviews* **113**, 303–341.

Wilkinson, J. J. (2013). Triggers for the formation of porphyry ore deposits in magmatic arcs. *Nature Geoscience* **6**, 917–925.

Windley, B. F., Alexeiev, D., Xiao, W. J., Kroner, A. & Badarch, G. (2007). Tectonic models for accretion of the Central Asian Orogenic Belt. *Journal of the Geological Society* **164**, 31–47.

Wu, F. Y., Sun, D. Y., Ge, W. C., Zhang, Y. B., Grant, M. L., Wilde, S. A. & Jahn, B. M. (2011). Geochronology of the Phanerozoic granitoids in northeastern China. *Journal of Asian Earth Sciences* **41**, 1–30.

Xiao, W. J., Huang, B. C., Han, C. M., Sun, S. & Li, J. L. (2010). A review of the western part of the Altaids: A key to understanding the architecture of accretionary orogens. *Gondwana Research* **18**, 253–273.

Xiao, W. J. & Santosh, M. (2014). The western Central Asian Orogenic Belt: A window to accretionary orogenesis and continental growth. *Gondwana Research* **25**, 1429–1444.

Xiao, W. J., Windley, B. F., Huang, B. C., Han, C. M., Yuan, C., Chen, H. L., Sun, M., Sun, S. & Li, J. L. (2009a). End-Permian to mid-Triassic termination of the accretionary processes of the southern Altaids: implications for the geodynamic evolution, Phanerozoic continental growth, and metallogeny of Central Asia. *International Journal of Earth Sciences* **98**, 1189–1217.

Xiao, W. J., Windley, B. F., Sun, S., Li, J. L., Huang, B. C., Han, C. M., Yuan, C., Sun, M. & Chen, H. L. (2015). A tale of amalgamation of three Permo-Triassic collage systems in central Asia: Oroclines, sutures, and terminal accretion. *Annual Review of Earth and Planetary Sciences* **43**, 477–507.

Xiao, W. J., Windley, B. F., Yuan, C., Sun, M., Han, C. M., Lin, S. F., Chen, H. L., Yan, Q. R., Liu, D. Y., Qin, K. Z., Li, J. L. & Sun, S. (2009b). Paleozoic multiple subduction-accretion processes of the southern Altaids. *American Journal of Science* **309**, 221–270.

Xie, L., Yin, H. Q., Zhou, H. R. & Zhang, W. J. (2014). Permian radiolarians from the Engeerwusu suture zone in Alxa area of Inner Mongoliaand its geological significance. *Geological Bulletin of China* **33**, 691–697.

Yakubchuk, A. (2004). Architecture and mineral deposit settings of the Altaid orogenic collage: a revised model. *Journal of Asian Earth Sciences* **23**, 761–779.

Yakubchuk, A., Degtyarev, K., Maslennikov, V., Wurst, A., Stekhin, A. & Lobanov, K. (2012). Tectonomagmatic settings, architecture, and metallogeny of the Central Asian copper province. *Society of Economic Geologists, Special Publication* **16**, 403–432.

Zhang, D. H. & Audétat, A. (2017). What caused the formation of the giant Bingham Canyon porphyry Cu–Mo-Au deposit? Insights from melt inclusions and magmatic sulfides. *Economic Geology* **112**, 221–244.

Zhang, S. H., Zhao, Y., Kroner, A., Liu, X. M., Xie, L. W. & Chen, F. K. (2009). Early Permian plutons from the northern North China Block: constraints on continental arc evolution and convergent margin magmatism related to the Central Asian Orogenic Belt. *International Journal of Earth Sciences* **98**, 1441–1467.